Theory of the Symmetrical Super-Condensed Node for the TLM Method

Vladica Trenkic, Christos Christopoulos, *Member, IEEE,* and Trevor M. Benson

***Abstract*—This paper describes a novel time-domain node for the TLM method. It has the unique feature of modeling arbitrary inhomogeneous media on a generally graded rectangular TLM mesh without using stubs. Variations in material properties and arbitrary aspect ratios of mesh cells are modeled by allowing different characteristic impedances in a cell, maintaining impulse synchronism throughout the mesh. The complete theory of the new node is given and its implementation on a general TLM mesh is discussed. Numerical results for a canonical resonator loaded with dielectric layers are presented for different grading cases. Substantial savings in computer storage and run-time as well as improved accuracy compared to the uniform mesh are achieved when an appropriate nonuniform grading of the TLM mesh is used.**

I. Introduction

IN CONVENTIONAL TLM schemes [1], [2], the characteristic impedance of interconnected transmission lines (also called link lines) is kept constant and equal to Z_0, the intrinsic impedance of the background medium. This ensures that the propagation delay remains constant and synchronism is maintained throughout the mesh. Variations in material properties and different cell aspect ratios are accounted for by introducing stubs [2] to slow down the propagation of pulses in the mesh.

In order to overcome difficulties imposed by the very unfavorable time steps required in a mesh using a graded symmetrical condensed node (SCN) [2], the hybrid symmetrical condensed node (HSCN) was introduced [3]. In the HSCN only capacitive stubs are required, since all inductance is modeled in the link lines resulting in three different values of characteristic impedance.

A number of papers discussing the use of different characteristic impedances of link lines inside a single cell were published recently. Hoefer and Sautier [4] have shown that a 2D-TLM network with the cells of arbitrary aspect ratio can be modeled by altering the characteristic impedances of transmission lines. In this scheme, different dielectric layers can be modeled by adjusting the mesh aspect ratio. An extension of this model to the 3D expanded (distributed) node was shown by Zhang and Hoefer [5]. Although these nodes are capable of modeling a variety of structures, it is not shown how different gradings can be used over a single dielectric layer and a uniformly graded mesh over different layers.

Manuscript received August 12, 1994; revised December 7, 1994. This work was supported by the Engineering and Physical Sciences Research Council, UK.

The authors are with the Department of Electrical and Electronic Engineering, University of Nottingham, NG7 2RD Nottingham, UK.

IEEE Log Number 9410715.

In a recently introduced frequency-domain TLM (FD-TLM) node [6] the characteristic impedance of link lines is also constant but variations in electrical properties are accounted for by modifying the phase constants of the lines. However, dispersion in the FD-TLM may be reduced by using a 'distributed' node with transmission lines of different characteristic impedance [7].

The main obstacle in formulating an SCN consisting of different line characteristic impedances is the complexity of deriving a scattering matrix using the standard approach of demanding that this matrix is unitary. In [8] a simple and elegant way of obtaining the scattering matrix was described and this approach has been applied to the derivation of a Symmetrical Super-Condensed Node (SSCN) where there are no stubs but six different link line characteristic impedances are necessary. The basic properties of the SSCN together with information on run-time, storage, accuracy and propagation were presented in [9] for a uniform mesh and in [10] for a generally graded mesh.

In the present paper, the complete theory of a general SSCN for TLM will be given including a compact definition for the line parameters, an elegant form of the scattering equations, the optimization of scattering coefficients and the evaluation of maximum permissible time step. The implementation of the new SSCN in a general rectangular TLM mesh containing different regions of arbitrary gradings and material properties will be described, including the connection procedure, modeling of external boundaries, calculation of the output for all field components and excitation in the mesh. The SSCN TLM algorithm will be validated by performing the analysis of a canonical resonator loaded with layers of dielectric.

II. Theoretical Development of the SSCN

A symmetrical condensed node is shown in Fig. 1 with the notation of voltages in the form V_{isj} where i denotes direction and j polarization of the appropriate transmission line ($i, j \in \{x, y, z\}$ and $i \neq j$), while $s \in \{n, p\}$ indicates the position of the port on the negative (n) or positive (p) side assuming the origin of coordinates at the centre of the node.

The development that follows refers to a cuboid cell of space with arbitrary dimensions Δx, Δy, Δz and material properties $\varepsilon = \varepsilon_0 \varepsilon_r$, $\mu = \mu_0 \mu_r$. The characteristic impedances Z_{ij}, distributed capacitances C_{ij} and distributed inductances L_{ij} of the transmission lines in a node are marked so that the first index i shows the direction and the second index j the polarization of the line ($i \neq j$). The lines with the same direction and polarization at a node have identical

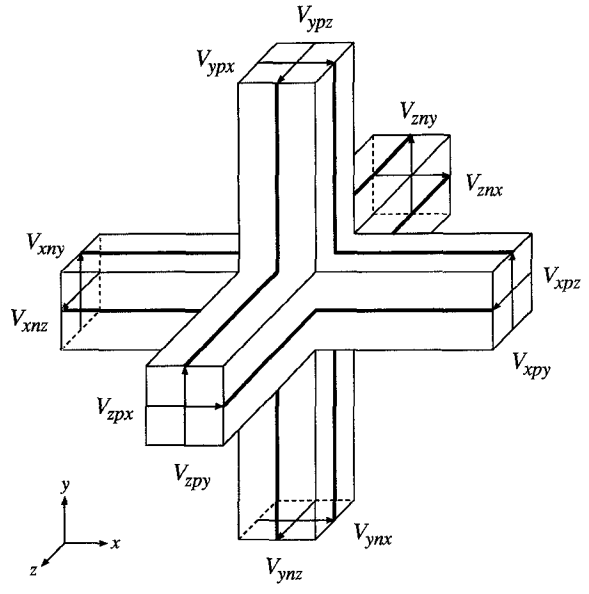

Fig. 1. Symmetrical condensed node.

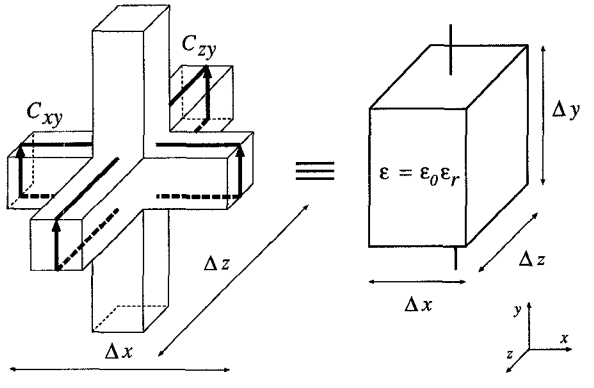

Fig. 2. Modeling capacitance in y-direction.

characteristics on either side of the node centre. This means that six different transmission line characteristic impedances are allowed in a 12-port node.

In the derivation of a TLM node capable of modeling a 3D space of arbitrary material properties on a generally graded mesh without using stubs, the following two basic conditions must be fulfilled:

1) The transmission lines in a node fully model the electromagnetic properties of the block of space represented by that node.
2) The transmission lines in a node allow the same propagation delay, Δt, in all directions.

A. Formulation of the System of Equations

The development starts by equating the electrical parameters of a cell to the transmission line parameters of the node. The total capacitance in, for example, the y-direction is illustrated in Fig. 2.

It can be seen from Fig. 2 that the cell's total capacitance C_y in the y-direction is represented by the distributed capacitance of two y-polarized transmission lines of the node. Thus, it follows that

$$C_{xy}\Delta x + C_{zy}\Delta z = \varepsilon\frac{\Delta z\Delta x}{\Delta y} \tag{1}$$

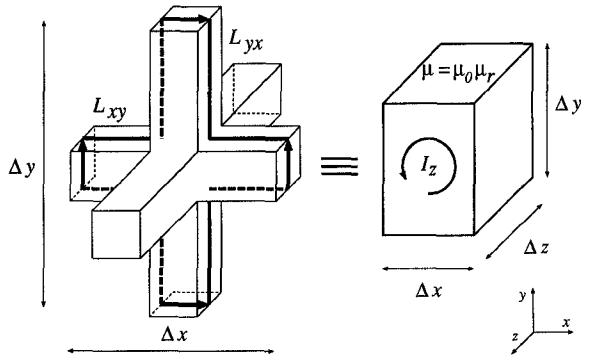

Fig. 3. Modeling inductance in z-direction.

where the left-hand side of (1) shows the total capacitance in the y direction contributed by the appropriate transmission lines, while the right-hand side shows the total capacitance in the same direction of the block of material modeled by the TLM cell. Similar equations can be obtained for the other two directions and summarized in a general form for the total capacitance C_k in the k direction

$$C_{ik}\Delta i + C_{jk}\Delta j = \varepsilon\frac{\Delta i\Delta j}{\Delta k} \tag{2}$$

where $i, j, k \in \{x, y, z\}$ and $i \neq j \neq k$

The total inductance in, for example, the z-direction is illustrated in Fig. 3.

It can be seen from Fig. 3 that the cell's total inductance L_z in the z direction is represented by the distributed inductance of two transmission lines contributing to the magnetic field in the z direction. Thus, it follows that

$$L_{xy}\Delta x + L_{yx}\Delta y = \mu\frac{\Delta x\Delta y}{\Delta z} \tag{3}$$

where the left-hand side of (3) shows the total inductance in the z direction contributed by the appropriate transmission lines, while the right-hand side shows the total inductance in the same direction of the block of material modeled by the TLM cell. Similar equations can be obtained for the other two directions and summarized in a general form for the total inductance L_k in the k direction

$$L_{ij}\Delta i + L_{ji}\Delta j = \mu\frac{\Delta i\Delta j}{\Delta k} \tag{4}$$

where $i, j, k \in \{x, y, z\}$ and $i \neq j \neq k$

In order to maintain time synchronism in the TLM mesh, the propagation delay Δt must be kept constant on all lines at every node in the mesh. The pulse velocity on the line ij is

$$v_{ij} = \frac{\Delta i}{\Delta t} = \frac{1}{\sqrt{C_{ij}L_{ij}}} \tag{5}$$

and the propagation delay Δt can be expressed as

$$\Delta t = \Delta i\sqrt{C_{ij}L_{ij}} \tag{6}$$

where indices i, j can take all possible combination of x, y, z giving a set of six equations.

The three equations obtained from (2), the three equations obtained from (4), and the six equations obtained from (6) form a system of twelve equations with the distributed capacitance and inductance of the six transmission lines as the

twelve unknowns. This is a nonlinear system of equations, but an analytical solution can be found as shown in the next subsection.

B. Derivation of Link Line Parameters

To express (2) and (4) in a more elegant form, we introduce normalized parameters for the link lines. For the pulse polarized in the j direction and propagating in the i direction, the medium distributed capacitance C_{ij}^m, the medium distributed inductance L_{ij}^m and the medium characteristic impedance Z_{ij}^m are

$$C_{ij}^m = \frac{C_j}{\Delta i} = \varepsilon \frac{\Delta k}{\Delta j} \tag{7}$$

$$L_{ij}^m = \frac{L_k}{\Delta i} = \mu \frac{\Delta j}{\Delta k} \tag{8}$$

$$Z_{ij}^m = \sqrt{\frac{L_{ij}^m}{C_{ij}^m}} = \sqrt{\frac{\mu}{\varepsilon}} \frac{\Delta j}{\Delta k}. \tag{9}$$

It is convenient to normalize the parameters of the link line to those of the block of medium, so we define the normalized distributed capacitance $\hat{C}_{ij}$, the normalized distributed inductance $\hat{L}_{ij}$ and the normalized characteristic impedance $\hat{Z}_{ij}$ of the i-directed j-polarized link line, respectively, as

$$\hat{C}_{ij} = \frac{C_{ij}}{C_{ij}^m} = \frac{C_{ij}}{\varepsilon} \frac{\Delta j}{\Delta k} \tag{10}$$

$$\hat{L}_{ij} = \frac{L_{ij}}{L_{ij}^m} = \frac{L_{ij}}{\mu} \frac{\Delta k}{\Delta j} \tag{11}$$

$$\hat{Z}_{ij} = \frac{Z_{ij}}{Z_{ij}^m} = \sqrt{\frac{\hat{L}_{ij}}{\hat{C}_{ij}}}. \tag{12}$$

We also introduce the *equivalent cubic cell parameter*, Δl, which actually represents the dimension of a cubic cell having the same propagation delay Δt as an arbitrarily graded TLM cell [4]. The velocity v of a pulse propagating along a transmission line in the SCN is twice the plane wave velocity in the medium with properties ε, μ [2] and is given by

$$v = \frac{\Delta l}{\Delta t} = \frac{2}{\sqrt{\varepsilon \mu}}. \tag{13}$$

Thus, Δl is given by

$$\Delta l = \frac{2\Delta t}{\sqrt{\varepsilon \mu}}. \tag{14}$$

Multiplying (2) by $\Delta k/(\varepsilon \Delta i \Delta j)$ and using (10) we obtain

$$\hat{C}_{ik} + \hat{C}_{jk} = 1 \tag{15}$$

Multiplying (4) by $\Delta k/(\mu \Delta i \Delta j)$ and using (11) we obtain

$$\hat{L}_{ij} + \hat{L}_{ji} = 1 \tag{16}$$

Using (10), (11), and (14), the general equation (6) can also be rewritten in terms of the equivalent cubic cell and normalized link line parameters as

$$\Delta l = 2\Delta i \sqrt{\hat{C}_{ij} \hat{L}_{ij}}. \tag{17}$$

We now solve a system of 12 equations (15)–(17) with 12 unknowns $\hat{C}_{ij}$ and $\hat{L}_{ij}$.

Taking $\hat{L}_{ij}$ from (17) for all possible combinations of $i, j \in \{x, y, z\}$ and substituting in (16) we obtain three equations of the general form

$$\frac{(\Delta l)^2}{4\hat{C}_{ij}(\Delta i)^2} + \frac{(\Delta l)^2}{4\hat{C}_{ji}(\Delta j)^2} = 1. \tag{18}$$

Substituting $\hat{C}_{ji}$ in (18) using an instance of (15) and dividing (18) by $(\Delta l)^2/4$ we obtain

$$\frac{1}{\hat{C}_{ij}(\Delta i)^2} + \frac{1}{(1 - \hat{C}_{ki})(\Delta j)^2} = \frac{4}{(\Delta l)^2}. \tag{19}$$

Substituting triplets (i, j, k) in (19) with (x, y, z), (y, z, x) and (z, x, y) respectively, we obtain a system of three equations with three unknowns $\hat{C}_{xy}, \hat{C}_{yz}, \hat{C}_{zx}$, which has a solution of the form

$$\hat{C}_{ij} = \frac{2(\Delta j)^2(\Delta k)^2 + B}{2(\Delta i)^2(\Delta k)^2[(2\Delta j/\Delta l)^2 - 1]} \tag{20}$$

where

$$B = A \pm \sqrt{A^2 - (\Delta x \Delta y \Delta z \Delta l)^2} \tag{21}$$

with

$$A = (\Delta x \Delta y \Delta z)^2 \left(\frac{4}{(\Delta l)^2} - \sum_{s=x,y,z} \frac{1}{(\Delta s)^2} \right). \tag{22}$$

The other three normalized capacitances, namely $\hat{C}_{xz}$, $\hat{C}_{yx}$ and $\hat{C}_{zy}$, can be found using (15). Note from (21) that there are two sets of solutions for the link line parameters of the SSCN. Both solutions are physical and either can be used in the definition of the SSCN. The preliminary testing of the two sets of parameters in the SSCN TLM simulations showed that they are equivalent within the frequency band of interest.

The normalized characteristic impedance $\hat{Z}_{ij}$ and the actual characteristic impedance Z_{ij} are obtained using (17), (12), and (9) as

$$\hat{Z}_{ij} = \frac{\Delta l}{2\Delta i \hat{C}_{ij}} \tag{23}$$

$$Z_{ij} = \hat{Z}_{ij} Z_{ij}^m = \frac{\Delta j}{\Delta i \Delta k} \frac{\Delta l}{2\hat{C}_{ij}} \sqrt{\frac{\mu}{\varepsilon}}. \tag{24}$$

For the benefit of later derivations we also solve the system of (15)–(17) directly in terms of $\hat{L}_{ij}$.

Taking $\hat{C}_{ij}$ from (17) for all possible combinations of $i, j \in \{x, y, z\}$ and substituting in (15) we obtain three equations of the general form

$$\frac{(\Delta l)^2}{4\hat{L}_{ik}(\Delta i)^2} + \frac{(\Delta l)^2}{4\hat{L}_{jk}(\Delta j)^2} = 1. \tag{25}$$

Substituting $\hat{L}_{jk}$ in (25) using an instance of (16) and dividing (25) by $(\Delta l)^2/4$ we obtain

$$\frac{1}{\hat{L}_{ik}(\Delta i)^2} + \frac{1}{(1 - \hat{L}_{kj})(\Delta j)^2} = \frac{4}{(\Delta l)^2}. \tag{26}$$

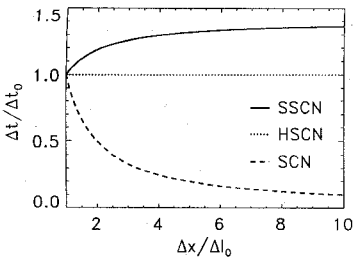

Fig. 4. Maximum time step for different nodes.

The system of equations (26) has a similar form to (19). Moreover, if we introduce the mapping $\hat{C}_{ij} \leftrightarrow \hat{L}_{ik}$ for all possible combinations of $i,j,k \in \{x,y,z\}$ the two systems of equations become equivalent, which leads to an important general relation for the symmetrical super-condensed node

$$\hat{C}_{ij} = \hat{L}_{ik} \tag{27}$$

which can be used for the optimization of scattering coefficients, as will be shown latter in this section.

C. Determination of the Maximum Permissible Time Step

So far, we have obtained the parameters of the link lines in terms of the linear dimensions of a node and the properties of the medium, but we have not yet determined the time step, or propagation delay, Δt, and accordingly the equivalent cubic cell parameter Δl which we have used in (20).

Analysing (20)–(22) and demanding that the characteristic impedance of a link line must be positive when modeling passive media [11], the following condition is imposed

$$A^2 - (\Delta x \Delta y \Delta z \Delta l)^2 > 0. \tag{28}$$

This condition can be used to determine the maximum permissible time step at a node. A cubic inequality has to be solved for $(\Delta l)^2$, giving one physical solution

$$\Delta l < \Delta l_{\max} = \frac{2}{C \cos\left[\frac{1}{3}\arccos(D/C^3)\right]} \tag{29}$$

where

$$C = \sqrt{\frac{4}{3}\sum_{s=x,y,z}\frac{1}{(\Delta s)^2}} \qquad D = \frac{8}{\Delta x \Delta y \Delta z}.$$

The maximum time step is then calculated using (14)

$$\Delta t_{\max} = \frac{\Delta l_{\max}\sqrt{\varepsilon\mu}}{2}. \tag{30}$$

A comparison of the maximum permissible time step in graded meshes for three different nodes, namely the stub-loaded SCN [2], the HSCN [3] and the SSCN, is made in Fig. 4. The node spacing in the y- and z-directions is fixed at $\Delta y = \Delta z = \Delta l_0$, while Δx varies from Δl_0 to $10\Delta l_0$. The maximum time step Δt is given relative to the time step Δt_0 used in a uniform mesh with node spacing Δl_0. It is clear from Fig. 4 that the time step allowed in the graded SSCN is consistently higher than for the HSCN and the stub-loaded SCN.

D. Scattering Properties of the SSCN

Scattering in the symmetrical super-condensed node can be derived from the principles explained in [8], without the need to explicitly enforce the unitary condition on the scattering matrix. The reflected voltages are described in terms of incident voltages and appropriate nodal voltages and loop currents. Using the notation formulated at the beginning of this section and bearing in mind that the parameters of a transmission line are identical on either side of the node centre, the scattering equations can be written in the form

$$V^r_{inj} = V_j + I_k Z_{ij} - V^i_{ipj} \tag{31}$$

$$V^r_{ipj} = V_j - I_k Z_{ij} - V^i_{inj} \tag{32}$$

where the node voltage V_j is

$$V_j = \frac{Z_{kj}}{Z_{ij}+Z_{kj}}(V^i_{inj}+V^i_{ipj}) + \frac{Z_{ij}}{Z_{ij}+Z_{kj}}(V^i_{knj}+V^i_{kpj}) \tag{33}$$

and the loop current I_k is

$$I_k = \frac{V^i_{ipj} - V^i_{inj} + V^i_{jni} - V^i_{jpi}}{Z_{ij}+Z_{ji}}. \tag{34}$$

Indices i,j,k take all possible combinations of x,y,z giving a set of 12 scattering equations which completely describe the scattering in the SSCN.

Using (24) and (17), the scattering coefficients appearing in formulae (31)–(34) can be expressed in terms of the normalized parameters of link lines

$$\frac{Z_{kj}}{Z_{ij}+Z_{kj}} = \hat{C}_{ij} \qquad \frac{Z_{ij}}{Z_{ij}+Z_{ji}} = \hat{L}_{ij}.$$

Therefore the node voltage V_j and the loop current I_k can be expressed in a more compact and physically meaningful form

$$V_j = \hat{C}_{ij}(V^i_{inj} + V^i_{ipj}) + \hat{C}_{kj}(V^i_{knj} + V^i_{kpj}) \tag{35}$$

$$I_k = \frac{\hat{L}_{ij}}{Z_{ij}}(V^i_{ipj} - V^i_{inj} + V^i_{jni} - V^i_{jpi}). \tag{36}$$

Replacing these expressions in the scattering equations (31) and (32) and using identities $\hat{L}_{ij} = \hat{C}_{ik}$ and $\hat{C}_{ij} = 1 - \hat{C}_{kj}$, the scattering coefficients used in the derivation of the original 12-port SCN scattering matrix [2] can be conveniently written as

$$a_{ij} = 1 - b_{ij} - d_{ij} \qquad b_{ij} = \hat{C}_{kj}$$

$$c_{ij} = d_{ij} - b_{ij} \qquad d_{ij} = \hat{C}_{ik}.$$

Indices i,j in coefficients $a-d$ denote the port voltages on the j-polarized i-directed line on either side of the node. The fact that both V_{inj} and V_{ipj} have the same scattering coefficients reflects the symmetrical property of the SSCN.

It can be readily checked that the scattering matrix $\mathbf{S}$ formed of coefficients described above satisfies the unitary condition given as $\mathbf{S}^{\mathrm{T}}\mathbf{Y}\mathbf{S} = \mathbf{Y}$ where $\mathbf{Y}$ is a 12×12 diagonal matrix with elements of the characteristic admittances of the 12 link lines. This also proves that the approach for obtaining scattering coefficients for a general TLM node given in [8] does conserve the energy in nodal scattering, even though this is not explicitly enforced by initial conditions.

III. Implementation of the SSCN in a TLM Mesh

We define the term *unique node region* as the region of TLM nodes describing the same material properties (ε_r, μ_r) on a part of the mesh where the cells are of constant linear dimensions $(\Delta x, \Delta y, \Delta z)$.

A. Time-Step in the SSCN TLM Mesh

In an actual implementation of the SSCN on a TLM mesh containing different dielectric layers and variable gradings, the time step in the mesh must be chosen as the smallest of all maximum permissible time steps calculated for separate node regions using (29) and (30). For example, when modeling two different materials, one with background properties (ε_0, μ_0) and another with the properties $(\varepsilon_r\varepsilon_0, \mu_r\mu_0)$ using the uniform mesh $(\Delta x = \Delta y = \Delta z = \Delta l_0)$, then we obtain from (29) identical maximum equivalent cubic cell dimensions equal to Δl_0, as expected. However, it can be shown from (30) that the maximum time steps for the two node regions differ by a factor $\sqrt{\varepsilon_r\mu_r}$ and the smaller one, corresponding to the background medium, must be used. Accordingly, the equivalent cubic mesh parameter for the material with properties $\varepsilon_r\varepsilon_0$, $\mu_r\mu_0$ becomes smaller, i.e. $\Delta l = \Delta l_0/\sqrt{\varepsilon_r\mu_r}$. This shows that in the TLM region modeling the medium whose electromagnetic properties are higher than the background ones, pulses travel more slowly, as expected.

B. Connection in the SSCN TLM Mesh

Inside a unique node region, the connection proceeds as in the usual SCN mesh, by simply swapping the pulses between adjacent ports of two neighboring nodes. This is valid since the characteristic impedance of a link line is the same on either side of the node.

Care must be taken at the interface between two different node regions where the characteristic impedance changes. A simple two-port junction must be modeled by calculating appropriate reflection and transmission coefficients, as explained in [4].

C. External Boundaries in the SSCN TLM Mesh

External boundaries of arbitrary reflection coefficient ρ_w may be modeled by terminating the link lines at the edge of the problem space with an appropriate load. The equivalent link line reflection coefficient, ρ_{ij}, generally differs from ρ_w and can be found as follows.

For a pulse polarized in the j direction travelling toward a boundary in the i direction, the characteristic impedance of the medium is Z_{ij}^m, and the resistance needed to terminate it in order to give reflection coefficient ρ_w is

$$R = Z_{ij}^m \frac{1+\rho_w}{1-\rho_w}. \tag{37}$$

The link line reflection coefficient, ρ_{ij}, is found by terminating the link line, of characteristic impedance Z_{ij}, with this same resistance

$$\rho_{ij} = \frac{R - Z_{ij}}{R + Z_{ij}} = \frac{(1+\rho_w) - \hat{Z}_{ij}(1-\rho_w)}{(1+\rho_w) + \hat{Z}_{ij}(1-\rho_w)} \tag{38}$$

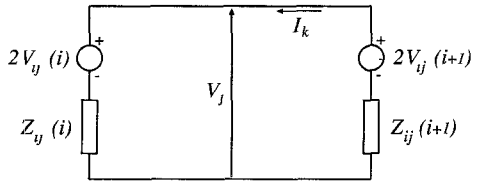

Fig. 5. Equivalent Thevenin circuit for finding voltage and current.

where the expression $Z_{ij} = \hat{Z}_{ij} Z_{ij}^m$ is used.

D. Output in the SSCN TLM Mesh

Electric and magnetic field components can be found from appropriate values of voltages and currents using

$$E_j = -\frac{V_j}{\Delta j} \qquad H_k = \frac{I_k}{\Delta k}.$$

Field values at a node can be readily obtained using formulae which define nodal voltages (35) and loop currents (36) already used in the scattering procedure.

In obtaining the output on link lines, the different characteristic impedances on interfaces between two node regions must be taken into account. Voltages and currents are found by solving the equivalent Thevenin circuit shown in Fig. 5

$$V_j = \frac{2[V_{ij}(i)Y_{ij}(i) + V_{ij}(i+1)Y_{ij}(i+1)]}{Y_{ij}(i) + Y_{ij}(i+1)} \tag{39}$$

$$I_k = \frac{2[V_{ij}(i+1) - V_{ij}(i)]}{Z_{ij}(i) + Z_{ij}(i+1)}. \tag{40}$$

If the output is required on a link line completely inside the unique node region, i.e. $Z_{ij}(i) = Z_{ij}(i+1)$, formulae (39) and (40) are simplified to

$$V_j = V_{ij}(i) + V_{ij}(i+1) \tag{41}$$

$$I_k = \frac{V_{ij}(i+1) - V_{ij}(i)}{Z_{ij}}. \tag{42}$$

E. Excitation in the SSCN TLM Mesh

If the excitation is specified in terms of field quantities, then the equivalent voltage pulses must be found. When exciting a particular field component, care must be taken not to excite others. This can be done if the electric charge and the magnetic flux are applied symmetrically to the node center.

In exciting the electric field component E_j, pulses must be injected into the mesh to give a total voltage $V_j = -E_j\Delta j$. From expression (35) and the charge symmetry conditions, the following ports need to be excited

$$V_{inj} = V_{ipj} = \frac{V_j}{4\hat{C}_{ij}} \qquad V_{knj} = V_{kpj} = \frac{V_j}{4\hat{C}_{kj}}.$$

From (35) and (36) it can be confirmed that all other nodal voltages and loop currents are zero, therefore only the desired field component is excited.

Similarly, for exciting the magnetic field component H_k, pulses must be injected into the mesh to give a loop current $I_k = H_k\Delta k$. Applying symmetry conditions for the magnetic

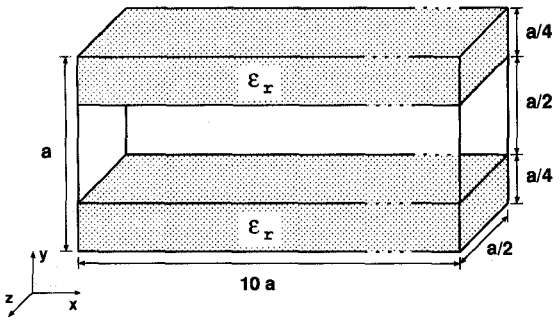

Fig. 6. Resonator loaded with dielectric layers of $\varepsilon_r = 4$ ($a = 7.112$ mm).

flux, it can be easily shown that the following voltage pulses need to be injected:

$$V_{ipj} = -V_{inj} = V_{jni} = -V_{jpi} = \frac{I_k Z_{ij}}{4\hat{L}_{ij}} = \frac{I_k Z_{ij}}{4\hat{C}_{ik}}.$$

For exciting field components on a link line, (39) and (40) with conditions, respectively, $I_k = 0$ and $V_j = 0$ can be used to obtain the values of voltages for the electric field E_j excitation

$$V_{ij}(i) = V_{ij}(i+1) = \frac{V_j}{2} \tag{43}$$

and the magnetic field H_k excitation

$$V_{ij}(i) = -\frac{I_k Z_{ij}(i)}{2} \tag{44}$$

$$V_{ij}(i+1) = \frac{I_k Z_{ij}(i+1)}{2}. \tag{45}$$

F. Implementation of Other Features in the SSCN TLM

A number of other features, e.g. internal boundaries, electrical and magnetic losses, thin features (wires, films, apertures), voltage and current sources, etc., can be implemented in the SSCN TLM. Procedures similar to the ones normally used in the SCN mesh can also be used in the SSCN mesh. Attention must be paid to the fact that the characteristic impedances of link lines in SSCN TLM differ in different node regions, and this should be dealt with in the implementation in a manner similar to the one used in the definition of outputs and excitation in the SSCN TLM mesh, described earlier in this section.

IV. Numerical Results

To validate the proposed TLM SSCN algorithm, we have modeled a canonical resonator loaded with dielectric, as illustrated in Fig. 6. Dielectric layers with relative permittivity $\varepsilon_r = 4$ are placed at the top and bottom of the cavity which is otherwise filled with free space ($\varepsilon_{r0} = 1$). Dimension a of the resonator is a =7.112 mm.

The benchmark resonant frequency for the TE_{110} mode, obtained by using two different TLM methods on a very fine uniform mesh, namely the SCN [2] and the SSCN, is $f_0 = 16.595$ GHz. Using the SSCN TLM method on a fine uniform mesh of 400 × 40 × 1 cells we have obtained $f =$ 16.584 GHz, which is 0.07% lower value than f_0. Note that appropriate excitation and short-circuit boundary conditions were used to reduce the number of cells in the z-direction, since for this particular mode there is no propagation in the z-direction.

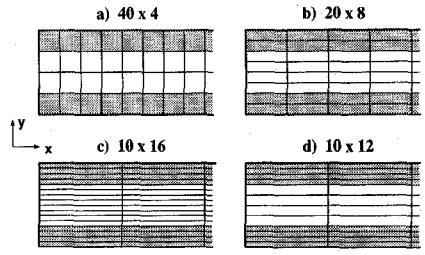

Fig. 7. Schematic of the different gradings of the TLM mesh.

We then used a coarse uniform mesh with 40 × 4 × 1 cells, part of which is illustrated in Fig. 7a and obtained a frequency of 15.480 GHz, underestimating f_0 by 6.72%. This inaccuracy occurred mainly because only one node per dielectric layer was used in the y-direction. The time step used in this simulation was $\Delta t_0 = 2.965$ ps.

Retaining the same number of cells, by increasing the node dimension in the x-direction by a factor of 2 and decreasing it by the same factor in the y-direction, as illustrated in Fig. 7(b), a uniformly graded mesh of 20 × 8 × 1 cells was used and the resonant frequency obtained was 16.322 GHz, i.e. 1.65% below the correct one. The time step was slightly decreased (0.899 Δt_0), but the number of cells and memory requirements remained the same and a more accurate result was achieved than in the case of the cubic cell mesh.

Further increase in aspect ratio, illustrated in Fig. 7(c) produced a mesh of dimension 10 × 16 × 1 cells and the simulated resonant frequency of 16.530 GHz was just 0.39% below the correct one. However, even though the same number of cells was used, the time step was decreased to $0.491\Delta t_0$.

So far, we have used only uniformly graded meshes to achieve the improvement in the modeled resonant frequency. Consider now a grading case when the grading in the y-direction within the dielectric is higher than in the region of free space. Since the propagation velocity in the dielectric is $\sqrt{\varepsilon_r} = 2$ times lower than in free space, we choose to grade that part of the mesh with twice as many cells. However, to maintain a reasonable number of cells, we increase node spacing in the free-space region, thus forming a mesh of 10 × 12 × 1 cells, part of which is shown in Fig. 7(d). The number of cells for this mesh was 25% smaller than in the previous case, the allowable time step was almost twice as high, namely $0.938\Delta t_0$, and the modeled frequency obtained was $f = 16.584$ GHz. This accuracy was the same as that achieved with a fine uniform mesh (400 × 40 × 1 cells). However the number of TLM cells used in the nonuniformly graded SSCN mesh was over hundred times smaller and the time step was almost 10 times higher than in the uniform case. By increasing the resolution of the nonuniformly graded SSCN mesh, by a factor of 2, i.e. using 20 × 24 × 1 cells, we obtained $f = 16.594$ GHz, an accuracy of better then 10^{-4}.

The summary of the results obtained for the different mesh configurations used is shown in Table I. It is clear from Table I that a uniformly graded mesh offers better results with less memory requirements than a uniform mesh, but that a nonuniformly graded mesh chosen in an appropriate manner shows even better characteristics.

TABLE I
CALCULATION OF TE_{110} FREQUENCY FOR DIFFERENT GRADING CASES ($f_0 = 16.595$ GHz)

Mesh	Freq. [GHz]	Error [%]	Time-step per Δt_0
U: 400 × 40	16.584	0.07	0.100
U: 40 × 4	15.480	6.72	1.000
G: 20 × 8	16.322	1.65	0.899
G: 12 × 12	16.476	0.72	0.645
G: 10 × 16	16.530	0.39	0.491
N: 10 × 12	16.584	0.07	0.938
N: 20 × 24	16.594	0.01	0.469

U—uniform mesh, G—Uniformly graded mesh, N—Nonuniformly graded mesh

V. CONCLUSION

A substantial development to the TLM method has been described, based on the symmetrical super-condensed node. The parameters and scattering properties of the node, its implementation including the maximum permissible time step, connection, boundaries, excitation and output, were described.

The use of normalized quantities presented in this paper enhances physical understanding and simplifies the derivation of line parameters and scattering properties of the SSCN. The standard SCN properties may be obtained as a special case of the SSCN described here, by substituting $\hat{C}_{ij} = 0.5$ and $\hat{Z}_{ij} = 1$ for all possible combinations of indices $i, j \in \{x, y, z\}$. The scattering matrix for the SSCN may be represented by only three quantities, e.g. $\hat{C}_{xy}, \hat{C}_{yz}, \hat{C}_{zx}$, by exploiting (15). The output, excitation and boundary conditions in the SSCN TLM must be treated especially to account for the fact that line impedances are not always the same.

The SSCN may be operated at a considerably higher time step than other nodes. The numerical example for a canonical resonator filled with dielectric layers reflected the versatility of the SSCN TLM scheme and showed its superiority in terms of computational requirements and accuracy. Further comparisons of this new implementation with other conventional implementations of the TLM method will be described in a future publication.

REFERENCES

[1] S. Akhtarzad and P. B. Johns, "The solution of Maxwell's equations in three space dimensions and time by the TLM method of numerical analysis," *Proc. Inst. Elec. Eng.*, vol. 122, no. 12, pp. 1344–1348, Dec. 1975.

[2] P. B. Johns, "A symmetrical condensed node for the TLM method," *IEEE Trans. Microwave Theory Tech.*, vol. MTT-35, no. 4, pp. 370–377, Apr. 1987.

[3] R. A. Scaramuzza and A. J. Lowery, "Hybrid symmetrical condensed node for TLM method," *Electron. Lett.*, vol. 26, no. 23, pp. 1947–1949, Nov. 1990.

[4] W. J. R. Hoefer and P. Sautier, "Characteristics of the general rectangular 2-D TLM network," *Int. J. Num. Modeling*, vol. 7, no. 2, pp. 127–139, Mar. 1994.

[5] Q. Zhang and W. J. R. Hoefer, "Characteristics of 3-D distributed node TLM mesh with cells of arbitrary aspect ratio," in *IEEE Int. Microwave Symp. Dig.*, San Diego, CA, May 23–27, 1994, pp. 369–372.

[6] D. P. Johns *et al.*, "New TLM technique for steady-state field solution in three dimensions," *Electron. Lett.*, vol. 28, no. 18, pp. 1692–1694, Aug. 1992.

[7] D. P. Johns, "An improved node for frequency-domain TLM—The 'distributed node'," *Electron. Lett.*, vol. 30, no. 6, pp. 500–502, Mar. 1994.

[8] V. Trenkic, C. Christopoulos, and T. M. Benson, "Simple and elegant formulation of scattering in TLM nodes," *Electron. Lett.*, vol. 29, no. 18, pp. 1651–1652, Sept. 1993.

[9] ——, "New symmetrical super-condensed node for the TLM method," *Electron. Lett.*, vol. 30, no. 4, pp. 329–330, Feb. 1994.

[10] ——, "Generally graded TLM mesh using the symmetrical super-condensed node," *Electron. Lett.*, vol. 30, no. 10, pp. 795–797, May 1994.

[11] D. A. Al-Mukhtar and J. E. Sitch, "Transmission-line matrix method with irregularly graded space," *IEE Proc.*, pt. H, vol. 128, no. 6, pp. 299–305, Dec. 1981.

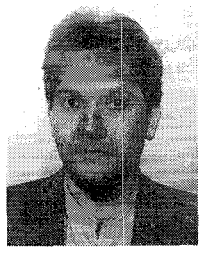

Vladica Trenkic was born in Aleksinac, Yugoslavia, in 1968. He received the Dipl. Ing. degree in electrical engineering with computer science from the University of Niš, Yugoslavia, in 1992, with an average mark 9.94 out of 10.

Since then he has been a research assistant in the Department of Electrical and Electronic Engineering at the University of Nottingham, England, where he is currently reading for a Ph.D. His research interests include numerical modeling using the transmission line modeling method and its implementation to electromagnetic compatibility and microwave heating problems.

Christos Christopoulos (M'92) was born in Patras, Greece, in 1946. He received the diploma in electrical and mechanical engineering from the National Technical University of Athens in 1969, and the M.Sc. and D.Phil. degrees from the University of Sussex in 1970 and 1975, respectively.

In 1974, he joined the Arc Research Project of the University of Liverpool and spent two years working on vacuum arcs and breakdown while on attachment to the UKAEA Culham Laboratories. In 1976, he joined the University of Durham as a senior demonstrator in Electrical Engineering Science. In October 1978, he joined the Department of Electrical and Electronic Engineering, University of Nottingham, where he is now professor of electrical engineering. His research interests are in electrical discharges and plasmas, electromagnetic compatibility, electromagnetics, and protection and simulation of power networks.

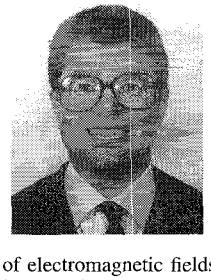

Trevor M. Benson, born in 1958, received the first-class honors degree in physics and the Clark Prize in Experimental Physics from the University of Sheffield in 1979 and the Ph.D. degree from the same university in 1982.

After spending over six years as a lecturer at University College, Cardiff, he joined the University of Nottingham as a senior lecturer in electrical and electronic engineering in 1989 and was promoted to the post of reader in 1994. His current research interests include experimental and numerical studies of electromagnetic fields and waves with particular emphasis on propagation in optical waveguides and electromagnetic compatibility.